View metadata, citation and similar papers at core.ac.uk
brought to you by CORE
provided by NASA Technical Reports Server

Final report for

Retrieval and Validation of Cirrus Cloud Properties with the Far-Infrared Sensor for Cirrus (FIRSC) During CRYSTAL-FACE

NASA grant NAG5-11501 to the University of Colorado, Boulder

Reporting period: 1/1/02 - 12/31/04

Principal Investigator: K. Franklin Evans
Program in Atmospheric and Oceanic Sciences
University of Colorado 311 UCB
Boulder, CO 80309
phone: 303-492-4994
email: evans@nit.colorado.edu

1. Overview

This grant supported the principal investigator's analysis of data obtained during CRYSTAL-FACE by two submillimeter-wave radiometers: the Far-Infrared Sensor for Cirrus (FIRSC) and the Conical Scanning Submillimeter-wave Imaging Radiometer (CoSSIR). The PI led the overall FIRSC investigation, though Co-I Michael Vanek led the instrument component at NASA Langley. The overall CoSSIR investigation was led by James Wang at NASA Goddard, but the cirrus retrieval and validation was performed at the University of Colorado. The goal of this research was to demonstrate the submillimeter-wave cirrus cloud remote sensing technique, provide retrievals of ice water path (IWP) and median mass particle diameter (D_{me}), and perform validation of the cirrus retrievals using other CRYSTAL-FACE datasets.

2. CoSSIR Portion of the Investigation

CoSSIR is a microwave radiometer which operated with a total of 12 channels: horizontally polarized channels at 183.3±1, 183.3±3, 183.3±6.6, 220, 380±0.8, 380±1.8, 380±3.3, 380±6.2, and 640 GHz, and vertically polarized channels at 487±0.7, 487±1.2, 487±3.3. The 183 and 380 GHz channels around water vapor lines provide water vapor profiling capability, while the 487 GHz channels around an oxygen line give upper troposphere temperature information. All channels are useful for cirrus IWP and D_{me} retrievals. The channels have matched beamwidths of about 4°. CoSSIR's two-axis scan mechanism was set up to perform cross-track scans. CoSSIR flew in a superpod of the ER-2.

CoSSIR suffered numerous failures during the CRYSTAL-FACE deployment. CoSSIR did operate during flights on July 1, 3, 7, 28, 29, 30 (the first and last being transit flights). The only flight in which the 487 GHz channels operated was on July 1. The only flight in which the 380 GHz channels operated properly was on July 28, though some of those channels were usable on other flights as well. The 640 GHz noise level was determined to be 6 to 16 K (depending on flight), which was much higher than anticipated. Many of the channels suffered from occasional noise spikes. The 183 GHz and 220 GHz channels were quite robust and low noise.

The focus of the CoSSIR data analysis was on performing retrievals of IWP and D_{me} and comparing with 94 GHz Cloud Radar System (CRS) data. A substantial effort was made to develop improved prior information for the Bayesian ice cloud retrieval algorithm. Ice particle size distributions from the FSSP, 2D-C, and HVPS optical cloud probes on the Citation aircraft were converted to ice water content (IWC) and D_{me} using mass-diameter relationships tuned to match the counterflow virtual impactor (CVI) measurements of IWC. The resulting mean and covariance matrix of temperature, ln(IWC), and $\ln(D_{me})$ are the microphysical prior information input to the retrieval algorithm. The ice cloud top height and thickness statistics for the retrieval were obtained from the CRS. NWS and PARSL radiosondes provided the statistics of temperature and relative humidity input to the retrieval algorithm. The microwave scattering properties needed for the retrieval were computed using the discrete dipole approximation for random aggregates of plates and aggregates of frozen droplets. These particle shapes were chosen to match the complex irregular particles observed with the Cloud Particle Imager.

A Monte Carlo Bayesian algorithm was used to retrieve IWP and D_{me} from the available CoSSIR nadir brightness temperatures. The retrievals were tested by retrieving vertically integrated 94 GHz radar backscattering from the CoSSIR data, which was then compared to Cloud

Radar System (CRS) data. The integrated backscattering typically agreed to 1–2 dB for IWP from 1000 to 10,000 g/m^2, while for lower IWP the typical agreement was 3–5 dB, which is within the Bayesian error bars. Retrievals of integrated backscattering using only the 183 and 220 GHz CoSSIR channels had almost as good agreement due to the high noise on the submillimeter channels.

An algorithm was developed to retrieve profiles of ice water content (IWC) and D_{me} from the combination of CRS reflectivity profiles and CoSSIR brightness temperatures. A power law relation (IWC $= 10^{0.1p} Z_e^q$) is assumed between IWC and equivalent radar reflectivity (Z_e), but the p and q coefficients are retrieved for each column. The IWC and D_{me} profiles and p and q are retrieved in a Bayesian integration that effectively matches the simulated and observed CoSSIR brightness temperatures. The radiometer data adds additional information to the radar profile so that the retrieved IWC and D_{me} are no longer completely dependent as they are with a traditional IWC-Z_e relation. The median retrieved p and q over all flights both increase from the a priori values for the highest IWP clouds. The results from the combined radar-radiometer profile algorithm illustrate how the coefficients for radar only ice cloud retrieval methods could be tuned for particular cloud types using submillimeter radiometer data.

The poorly performing submillimeter-wave channels greatly reduced CoSSIR's sensitivity to thinner ice clouds, and thus comparison of CoSSIR retrievals with infrared radiometer measurements or combined retrievals were not deemed productive.

A paper was published describing the CoSSIR data analysis in detail:
Evans, K. F., J. R. Wang, P. E. Racette, G. Heymsfield, L. Li, 2005: Ice cloud retrievals and analysis with data from the Compact Scanning Submillimeter Imaging Radiometer and the Cloud Radar System during CRYSTAL-FACE. *J. Appl. Meteor.*, **44,** 839–859.

3. FIRSC Portion of the Investigation

FIRSC is a Fourier Transform Spectrometer (FTS) with a useful spectral range from 15 to 50 cm^{-1} (450 to 1500 GHz) at 0.2 cm^{-1} resolution. Its 0.3 K cooled bolometer detector requires daily filling with liquid nitrogen and liquid helium and a two hour ^{3}He pumping procedure before the detector is ready for flight. FIRSC is nadir viewing with a 0.03 radian field of view and takes a interferometer scan in 4 seconds. FIRSC flew on the Proteus aircraft with the NAST-M microwave radiometer and the NAST-I infrared interferometer.

3.1. Deployment activities

Mike Vanek and Frank Evans were in Key West for the whole month of the deployment, while Ira Nolt and Clare Lee were there for about 2.5 weeks each, at the beginning and end of the month, respectively. Vanek oversaw FIRSC operations, handled the FIRSC control software, and performed repairs. Nolt and Lee handled the FIRSC detector and cryogenics and helped with other aspects of the instrument operations. Evans analyzed the FIRSC data and also substituted for Bill Smith as the Proteus flight scientist when needed.

The FIRSC instrument suffered a number of failures and problems during the deployment. Due to a miscommunication the Proteus pilots turned off FIRSC during the ferry flight from California. As a result the instrument was cold soaked and its computer would not boot. FIRSC missed the first science flight while a new computer board was being delivered. FIRSC operated during the next

three Proteus flights on July 7, 9, and 11. On the July 11 flight FIRSC's port selection mirror failed to rotate back to the sky port after the mid flight calibration sequence, and so there is no data from the later portion of the flight. The FIRSC GPS did not operate during the deployment, perhaps due to the antenna being shared among the five instruments, and so the GPS location information was obtained from the NAST-I team. A FIRSC software timeout on the GPS error caused the FTS scans to be taken about every 12 seconds on the July 7 to 11 flights, instead of the usual every 6 seconds.

On the July 13 flight FIRSC never began taking data, for unknown reasons. On the July 16 flight FIRSC's breaker tripped upon power on, and the Proteus was called back to prevent potential damage to the instrument if the outside of the cryostat got too cold. Eventually the problem was traced to a damaged DC-to-DC converter in one of FIRSC's power supplies. A new part was ordered and installed to get FIRSC working again. While FIRSC was being repaired it missed the solo clear sky Proteus flight on July 17 and the mostly clear sky Proteus flight to Georgia on July 19. FIRSC operated successfully thereafter on the four remaining Proteus flights (Proteus did not fly on July 28 due to a failed engine starter/generator).

Table 1 lists the flights on which FIRSC operated, the number of brightness temperature spectra submitted to the archive, and the periods of these flights during which FIRSC took sky data. FIRSC calibration scans were taken in blocks of 100 scans (50 hot blackbody and 50 cold blackbody). The FIRSC calibration is quite stable, so the calibration scans do not need to be performed often, but a number of scans is required to reduce the noise on the calibration. The calibration sequence was to take 600 or 500 calibration scans at the start as the aircraft was climbing to altitude and the instrument was outgassing water vapor. The calibration scans at the beginning of the flight resulted in some loss of data, especially in the earlier flights when the scans were taken more than 6 seconds apart. There were also calibration scans performed during scans 1201-1300 and 2401-2500, and so there is usually one gap (10 minutes for 6 seconds between scans) in the middle of the flight. On July 11, 23, and 26 FIRSC shut down during the flight and was restarted when the pilots noticed the control lights had stopped flashing; thus these flights have an additional data gap. Before the July 21 flight, the FIRSC computer operating system was changed from Windows 2000 to Windows XP. The Windows shutdown sequence no longer completed before the power supply shutoff. This resulted in losing 14 to 88 minutes of data at the end of each flight.

We had intended to process the FIRSC interferograms to calibrated brightness temperature spectra and perform cirrus IWP and D_{me} retrievals. However, it immediately became apparent that the noise on the FIRSC T_b spectra were much larger than we had anticipated. Instead of the T_b noise rms being roughly $\sigma_T = 1.0(30/\nu)^2$ it was roughly ten times larger (e.g. 40 K instead of 4 K at $\nu = 15$ cm^{-1}). This huge noise would make the FIRSC data in the crucial 22 cm^{-1} and 29 cm^{-1} windows unusable. This high noise level which had been discovered before the deployment, was the reason behind switching FIRSC from the original 0.1 cm^{-1} spectral resolution to 0.2 cm^{-1} . We spent much of the month investigating and discussing the cause of the noise and ways to deal with it. Unfortunately, we came to the conclusion that the underlying problem could not be fixed in the field, though there are ways of effectively reducing the noise.

A graph of the mean and standard deviation of the hot calibration blackbody interferograms (Fig 1) was a strong piece of evidence for the source of the noise problem. Since the blackbody target is constant, the standard deviation of the interferogram should be the detector noise level, which would be indistinguishable from zero on this graph. Instead there are peaks in standard

Table 1: FIRSC data status during CRYSTAL-FACE[a].

Flight	N spectra	Δ time	Operating periods (UTC sec)
July 7	536	12	64898-71976, 73187-78776
July 9	800	12	59846-66919, 68132-79972
July 11	300	13	60388-60979, 61324-68386
July 21	436	8	70402-75131, 75975-78114
July 23	898	6	68455-71461, 73151-74667, 75363-82353
July 26	886	6	66489-70334, 71051-71780, 72479-79481
July 29	900	6	62675-67004, 67690-74521

[a] N spectra is the number of spectra submitted to the CRYSTAL-FACE archive. Only the even FIRSC scans, which have lower noise, are submitted. Δ time is the approximate time in seconds between the beginning of FIRSC scans. FIRSC did not operate for Proteus flights on July 3, 13, 16, 17, and 19.

deviation where the interferogram is changing most rapidly. For this flight the maximum hot cal interferogram standard deviation is 15% of the interferogram peak (other flights have up to 24%). This pattern of standard deviation is consistent with errors in the interferometer mirror sampling position. The position encoder is on the shaft of the mirror drive motor, but the shaft is connected by a belt to a pulley on a lead screw which drives the mirror stage. The mirror stage is probably sticking which causes sudden jumps in the interferogram position (which we have seen in individual interferograms). Further evidence for this is that the even scan interferograms have considerably lower standard deviation than the odd scans ones, even though their means are the same. The odd scans have the mirror traveling in one direction, while the even scans have the mirror traveling in the opposite direction. Given the higher noise of the odd scans, we have decided to use only the even scans.

3.2. Post-deployment analysis

The first order of business was to deal with the high noise on the FIRSC spectra. The simplest and most effective technique is to exclude the odd scans. We tried a technique to shift back sections of the center part of the interferogram that appeared shifted by the sticky mirror travel. One technique that actually did offer some benefit was to perform a least squares fit to the interferograms rather than the usual straight Fourier transform. The reason the fitting technique provides a benefit is that we can impose the constraints that the raw spectra be real and that they contain no power above the cutoff filter (above around 60 cm^{-1}). The interferogram shifts from the sticky mirror cause spurious high frequencies in the spectrum. The raw spectrum values at 1.0 cm^{-1} resolution are adjusted to minimize the χ^2 interferogram fit measure using a conjugate gradient routine. The least squares fitting χ^2 includes the standard deviation estimate σ_i at each point i in the interferogram: $\chi^2 = \sum_i (S_i^{(sim)} - S_i^{(obs)})^2/\sigma_i^2$, where $S^{(sim)}$ is the interferogram simulated from the raw spectrum values and $S^{(obs)}$ is the FIRSC observed interferogram. The standard deviation estimate σ_i obtained from a constant scene, such as the hot calibration scans or clear sky. The fit is performed only to the inner portion of the interferogram where the mirror position sampling error is significant due to the large interferogram signal. The fitting procedure results in a corrected interferogram which is then processed in the usual manner.

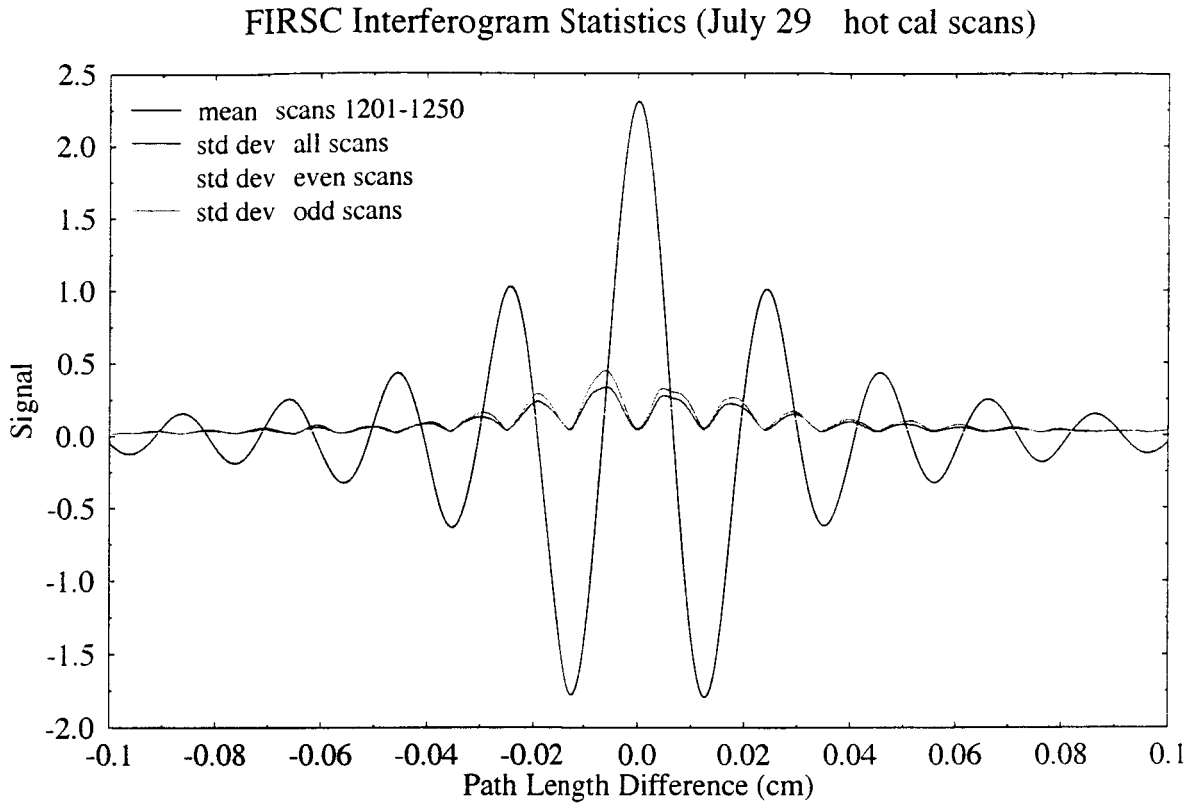

Figure 1: The mean and standard deviation of the inner portion of 50 hot calibration target interferograms. Also shown is the standard deviation of the even scan interferograms and the odd scan ones. The full interferogram runs between -2.5 and 2.5 cm optical path length difference.

Figure 2 shows the standard deviation of brightness temperature spectra for a clear sky period of FIRSC data processed by different methods. While there may be some variability in brightness temperature from water vapor and temperature variations, these would not increase at lower frequencies, and thus most of the variability is due to instrument noise. There is a large decrease in noise by simply excluding the odd scans. The interferogram fitting technique gives a modest, yet significant, further reduction in noise at the lower frequencies. The interferogram fitting method reduces the noise more in the all scan sample than for even scans only. Other flights have higher noise than the July 29 flight. Based on results like these we decided to use the interferogram fitting technique and only include the even FIRSC scans in the archived files. The noise is still higher than anticipated before the deployment, so we consider the usable spectral range to be 15 to 50 cm^{-1} , instead of the 10 to 47 cm^{-1} we had expected previously.

An example of the data from all of the July 29 flight is shown in Fig. 3. Brightness temperatures for radiances averaged over three spectral regions or "channels" are plotted as a function of time. The channels are centered in the three windows most important for cirrus remote sensing (channel bandpasses are 21.0-23.6 cm^{-1} , 28.2-30.0 cm^{-1} , and 44.4-46.0 cm^{-1}). The top panel shows that the lower frequency data are unusable if the odd scans are not editted out. The early part of the flight, before the calibration gap, was in clear sky or over low clouds that the submillimeter

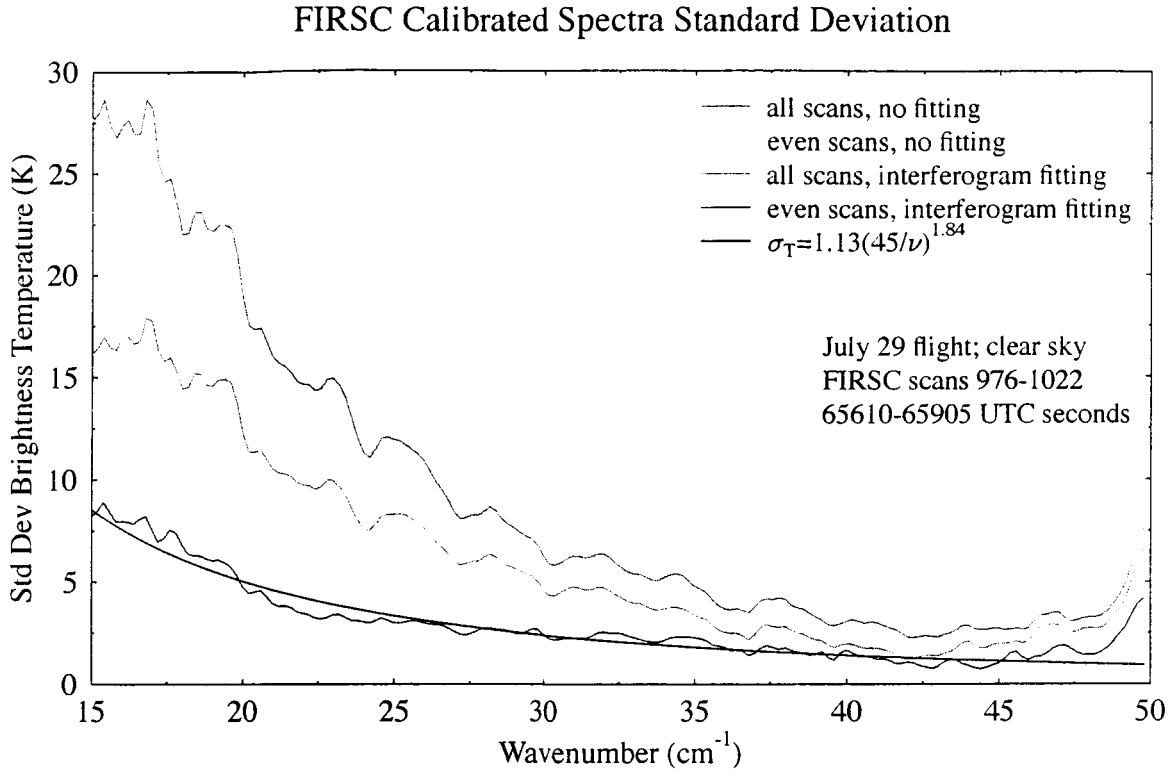

Figure 2: The standard deviation of brightness temperature spectra for four processing methods for a short clear sky period during the July 29 flight.

radiometer does not detect. As expected from previous modeling the 22 cm^{-1} and 29 cm^{-1} T_b match in clear sky, while the 45 cm^{-1} T_b are about 10 K lower. During the latter part of the flight the Proteus repeatedly flew over a cirrus anvil and convective core. The 22 cm^{-1} and 29 cm^{-1} brightness temperatures drop to around 150 K in the convective cores, while the 45 cm^{-1} T_b decrease is smaller due to more absorption by the ice particles and water vapor. The T_b depression is sudden on the upwind side of the convection, but more gradual on the downwind side as the cirrus anvil slowly thins with distance from the convective core.

The analysis of FIRSC data concentrated on checking the absolute calibration using two methods: 1) comparing with the CoSSIR 640 GHz channel brightness temperature when the ER-2 and Proteus were colocated, and 2) comparing FIRSC spectra with modeled clear sky spectra from temperature and water vapor profiles retrieved by NAST-I and obtained from in situ water vapor measurements.

The July 29 flight had the only times FIRSC and CoSSIR were colocated during periods of no high clouds (so the submm T_b are relatively constant). During this flight there were only three colocations without ice clouds when the CoSSIR data is usable. Figure 4 compares the FIRSC and CoSSIR nadir 640 GHz brightness temperatures for the segment of the flight containing these three colocations. These three match ups are not ideal. The 64005 sec colocation is in a Proteus turn,

the 65830 sec time has the ER-2 and Proteus going in opposite directions, and the 66425 sec colocation has spikes in the CoSSIR 640 GHz T_b's. The figure does show relatively good agreement between the two radiometers when the separation distance is small. The comparison is quantified by averaging the FIRSC and CoSSIR brightness temperatures over time periods centered on the three colocated times (see Table 2). The CoSSIR data around 66425 sec has been editted by removing samples with $T_b > 265$ K. There is very good agreement between the FIRSC and CoSSIR 640 GHz mean brightness temperatures for these colocations. Around 65830 sec CoSSIR has a burst of downward spikes, which are likely to be noise, that explain the larger FIRSC - CoSSIR T_b difference for that colocation. There is also reasonably good agreement in the 640 GHz brightness temperatures during the two colocations over cirrus that occurred later in the flight (not shown), even though the T_bs are changing and the aircraft horizontal distance is greater than 2.5 km.

Table 2: Statistics of FIRSC and CoSSIR 640 GHz brightness temperatures for colocated times[b].

Times (UTC seconds)		FIRSC T_b			CoSSIR T_b			ΔT_b	pooled
Crossing	Range	mean	stddev	N	mean	stddev	N	(K)	stderr
64005	63705-64105	247.8	5.2	32	246.9	6.7	89	0.85	1.16
65830	65630-66030	245.9	4.2	32	242.4	7.2	89	3.51	1.07
66425	66175-66675	247.5	5.3	40	247.7	6.7	99	-0.15	1.07

[b] ΔT_b is the difference between the FIRSC and CoSSIR mean T_bs. The "pooled stderr" is the error in the difference of the means derived from the standard deviations ("stddev"). N is the number of samples being averaged.

The second check on the absolute calibration of FIRSC was to compare averaged FIRSC brightness temperature spectra with modeled spectra. NAST-I cloud retrievals were used to select 5 minute periods of clear sky during the flights on July 26 and 29. The NAST-I retrieved nadir pixel temperature and water vapor profiles were averaged over these periods. Clear sky submillimeter-wave brightness temperature spectra were computed from the NAST-I profiles with LBLRTM and rtspec models (using the same apodization function as for the FIRSC spectra). The first comparison showed the T_b spectra from the NAST-I profiles to be 5 to 15 K higher than the FIRSC spectra. Upon seeing these results Bill Smith decided to change the NAST-I retrieval procedure. The old NAST-I retrievals assumed that the radiosonde-based upper troposphere humidity statistics were correct and bias adjusted the retrievals. The new NAST-I retrievals don't perform this bias adjustment and are therefore more consistent with the NAST-I observed infrared radiances. The Harvard in situ water vapor data from the WB-57 were used to check the NAST-I water vapor profiles. The WB-57 and Proteus were colocated only when the WB-57 was at a few altitudes, and these are spread out over much of the flight. An in situ profile was obtained from the Harvard instrument using data from ascents and decents before 65000 sec UTC. Figure 5 shows the water vapor profiles from one clear sky period used in the modeling. The Harvard water vapor profile is consistent with ice saturation from 10 km to 13.5 km, but is much drier above. The new NAST-I water vapor profile does agree better than the old one, but is still too dry from 10 km to 14 km.

Figure 6 shows the comparison between FIRSC and modeled brightness temperature spectra for one 5 minute period. The FIRSC T_b spectrum for this period and most of the others agree best with spectrum modeled from the ice saturation profile. The T_b spectrum from the Harvard water vapor profile is slightly higher than the FIRSC spectrum, while the NAST-I spectrum is still considerably

higher than FIRSC. The sources of the disagreement could be errors in the FIRSC calibration, uncertainties in the NAST-I calibration or retrieval process, or errors in the LBLRTM/HITRAN spectroscopic data. Assuming the Harvard water vapor profile is the most accurate source of water vapor here, these results support our claim that the absolute accuracy of FIRSC spectra is within 3 K. However, further comparisons will be required to actually establish the absolute accuracy of FIRSC.

Figure 7 shows six measured spectra obtained during a single pass over an anvil on July 29. Each spectrum is is an average of about nine FIRSC spectra to reduce the noise. Also shown are two modeled spectra: one for clear sky and one for ice cloud parameters that have been roughly fit to match the measured spectrum. The FIRSC spectra agree reasonably well with the modeled spectra. There is a substantial brightness temperature depression in the 45 cm^{-1} window due to the high top ice cloud, though the depressions are larger for the 22 and 28 cm^{-1} windows.

Retrievals of cirrus ice water path and median mass equivalent sphere diameter were performed on all the even scan FIRSC data. These retrievals along with the input FIRSC brightness temperature spectra were submitted to the CRYSTAL-FACE archive (FI200207*_TB.PROT and FI200207*_IWP.PROT files). These retrievals use the Bayesian algorithm described in Evans et al. (2002, JGR, 10.1029/2001JD000709). The retrieval database contains 4×10^5 cases. For each case the temperature profile, relative humidity profile, ice cloud height and thickness, the ice water content (IWC) and median particle diameter (D_{me}) at the cloud top and bottom, particle gamma size distribution width, and particle shape are chosen randomly. The statistics of the temperature and relative humidity profile are derived from a covariance matrix of temperature and humdity at various levels computed from 25 radiosondes lauched during CRYSTAL-FACE. The cirrus microphysics statistics are derived from in situ 2DC probe observations of tropical cirrus anvils during CEPEX. The particle shapes are 4 and 7 bullet-rosettes and 50% density ice spheres. The cloud top height distribution is Gaussian with a mean of 12.7 km and a standard deviation of 1.2 km. The cirrus cloud thickness has an exponential distribution with a mean of 5.0 km. A FIRSC brightness temperature spectrum is simulated for each database case with a fast radiative transfer model. To reduce the dimensionality of the database the T_b in the spectra are transformed to EOF amplitudes using Empirical Orthogonal Function (EOF) analysis. Each case in the retrieval database contains the simulated EOF amplitudes and the desired retrieval parameters, IWP and D_{me}.

The Bayesian retrieval algorithm finds the cases in the database that roughly match the six EOF amplitudes calculated from the FIRSC T_b spectrum. The uncertainty of the EOF amplitudes is estimated for each flight using a set of FIRSC spectra for a constant scene such as a clear sky segment or hot calibration scans. The weighted sum of IWP and D_{me} is the mean of the posterior pdf, which is the minimum variance solution. The standard deviation of the posterior pdf is an estimate of the uncertainty of the retrieval.

Figure 8 shows the cirrus IWP and D_{me} retrieval for a portion of the July 29 flight. The retrieved ice water path increases almost linearly in time from 19.7 hours to 20 hours as the Proteus flew upwind along a cirrus anvil to the convective core. During this time the retrieved median particle diameter increased from 130 μm to 250 μm. The noise on the FIRSC spectra may cause the extremely large spikes in the thick parts of the anvil. The Bayesian derived error bars for IWP are very large in the thick anvil regions, which is due to FIRSC's lack of sensitivity to the lower frequencies that penetrate deeper in the anvil. Thus the poor quality of the FIRSC data cause the ice cloud retrievals to be of little use.

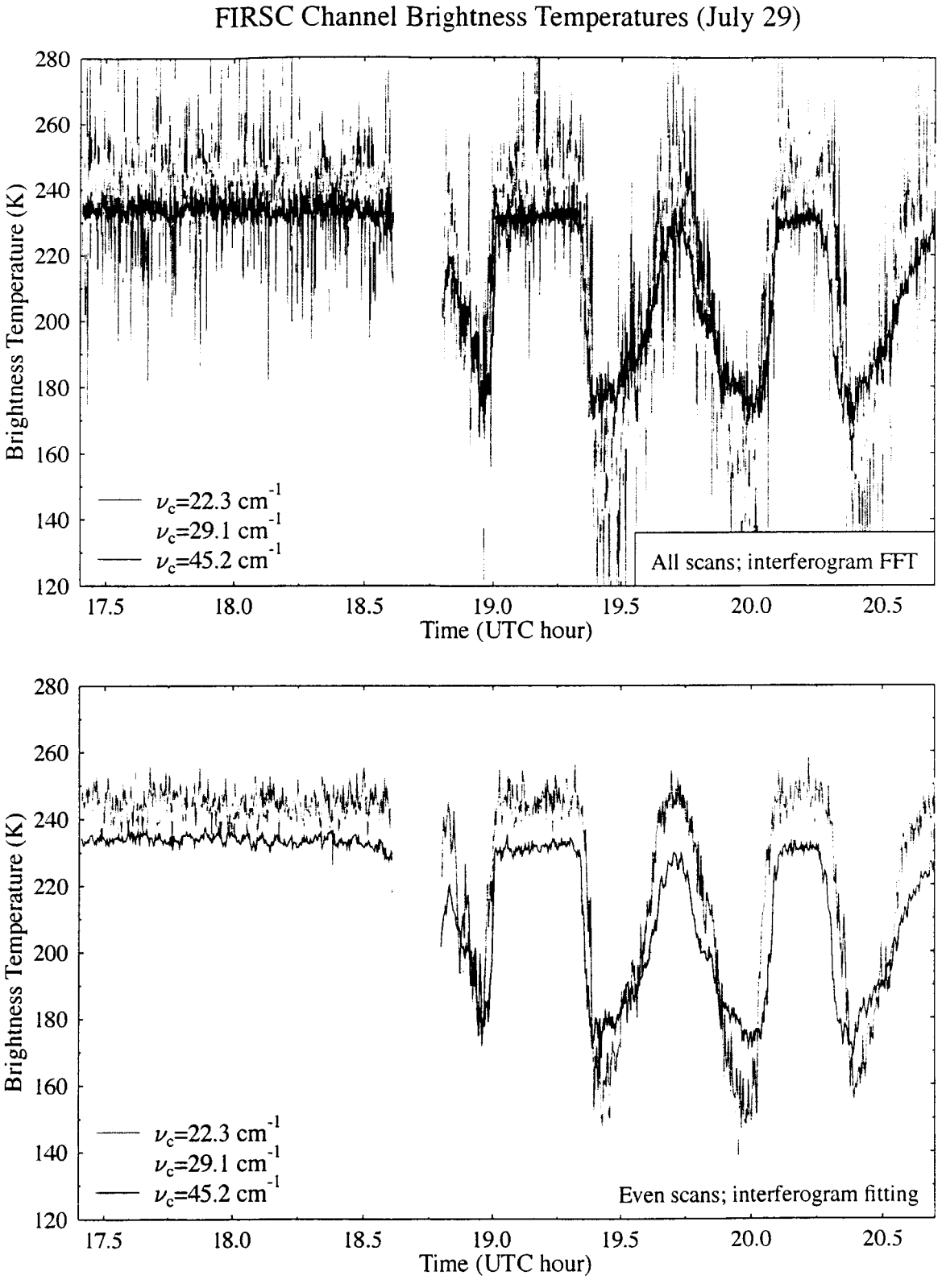

Figure 3: Brightness temperature for three channels made from FIRSC calibrated spectra.

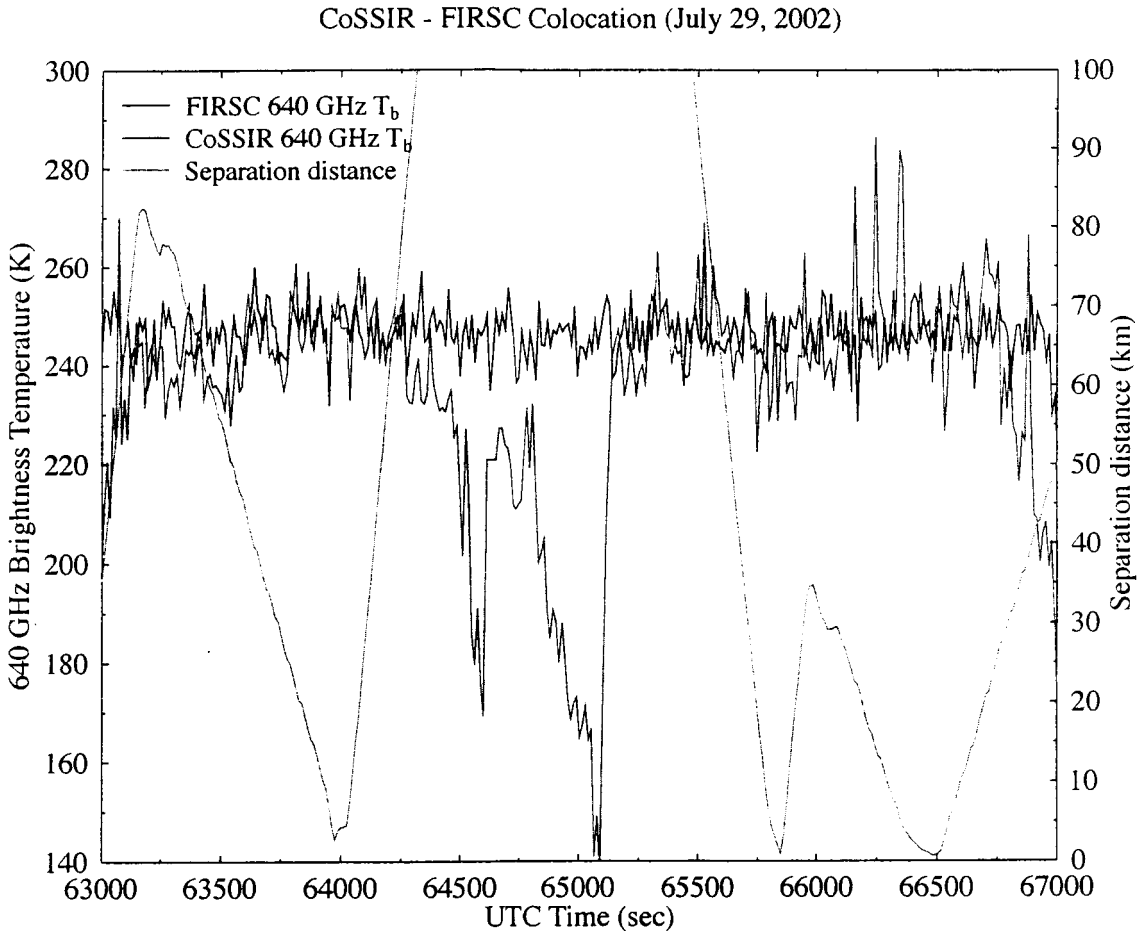

Figure 4: FIRSC and CoSSIR 640 GHz nadir brightness temperatures for colocated points (closest CoSSIR horizontal location within 30 seconds to each FIRSC scan). Also shown is the separation distance.

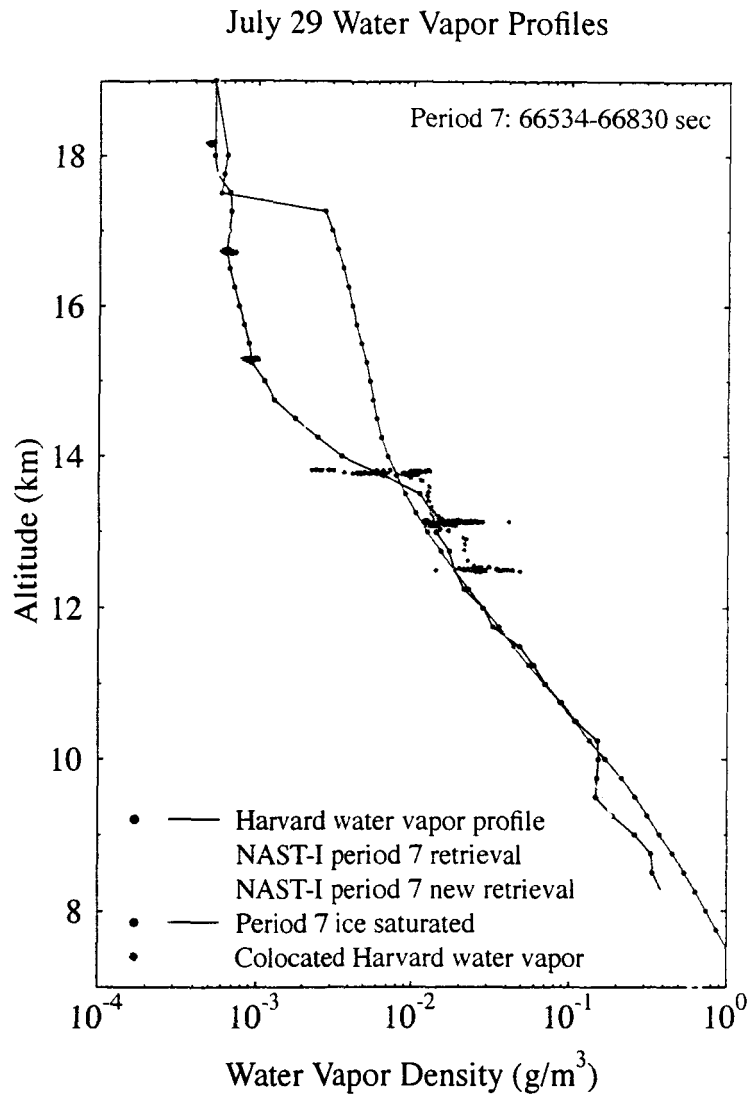

Figure 5: Water vapor density profiles used in the submillimeter T_b spectra modeling. The magenta points show the water vapor density from the Harvard instrument when the WB-57 was horizontally collocated with the Proteus within 30 km and 300 seconds. The two NAST-I profiles are averages over nadir pixel retrievals from the 5 minute period listed. The new NAST-I retrieval does not have the bias correction to agree with radiosonde statistics that the original NAST-I retrieval had. The ice saturation profile is calculated using the new NAST-I temperature profile.

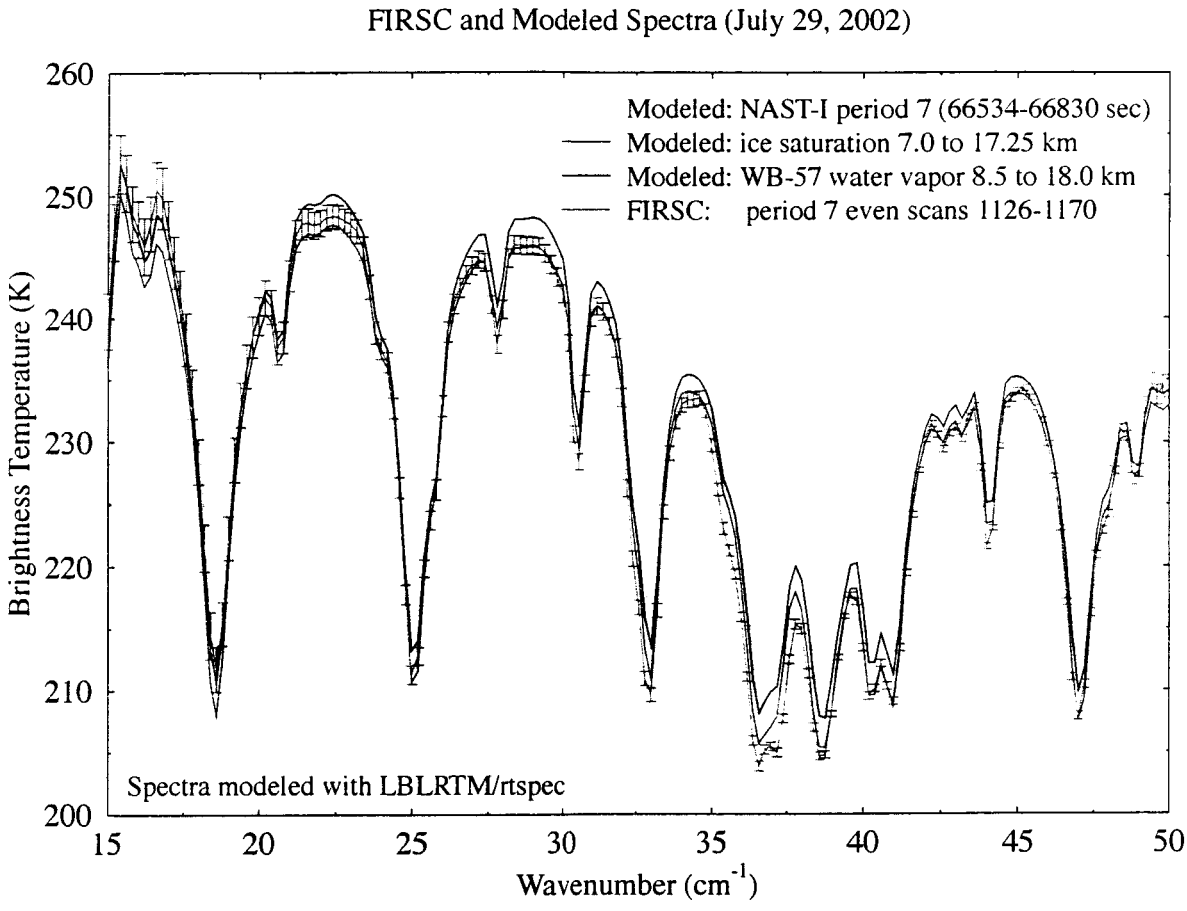

Figure 6: FIRSC and modeled brightness temperature spectra for a 5 minute period on July 29. The error bars show standard error of the mean over the 23 FIRSC spectra included in the average. The Proteus altitude was modeled at 17.25 km. The temperature profiles are from the new NAST-I retrieval.

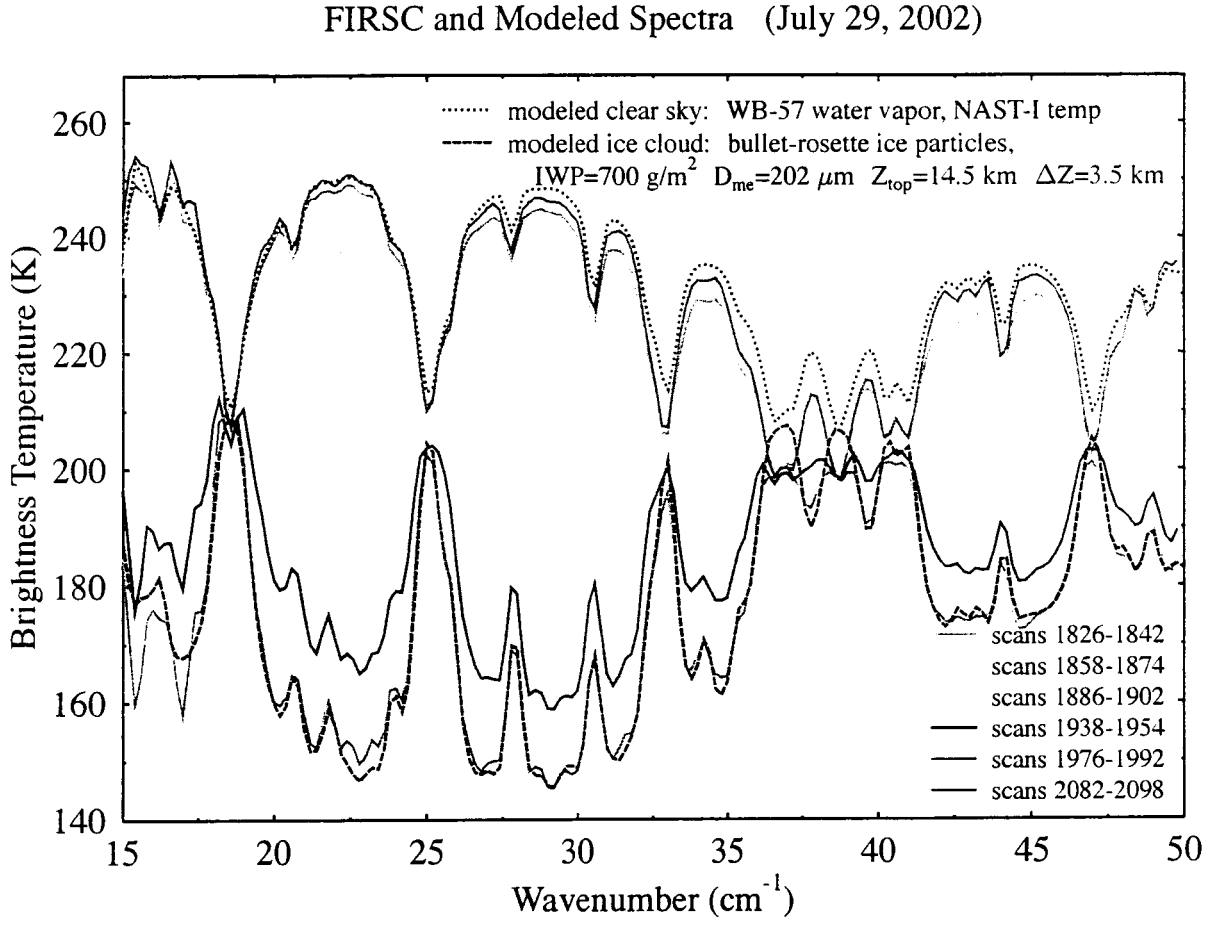

Figure 7: FIRSC and modeled brightness temperature spectra for selected averaged spectra across one anvil leg on July 29.

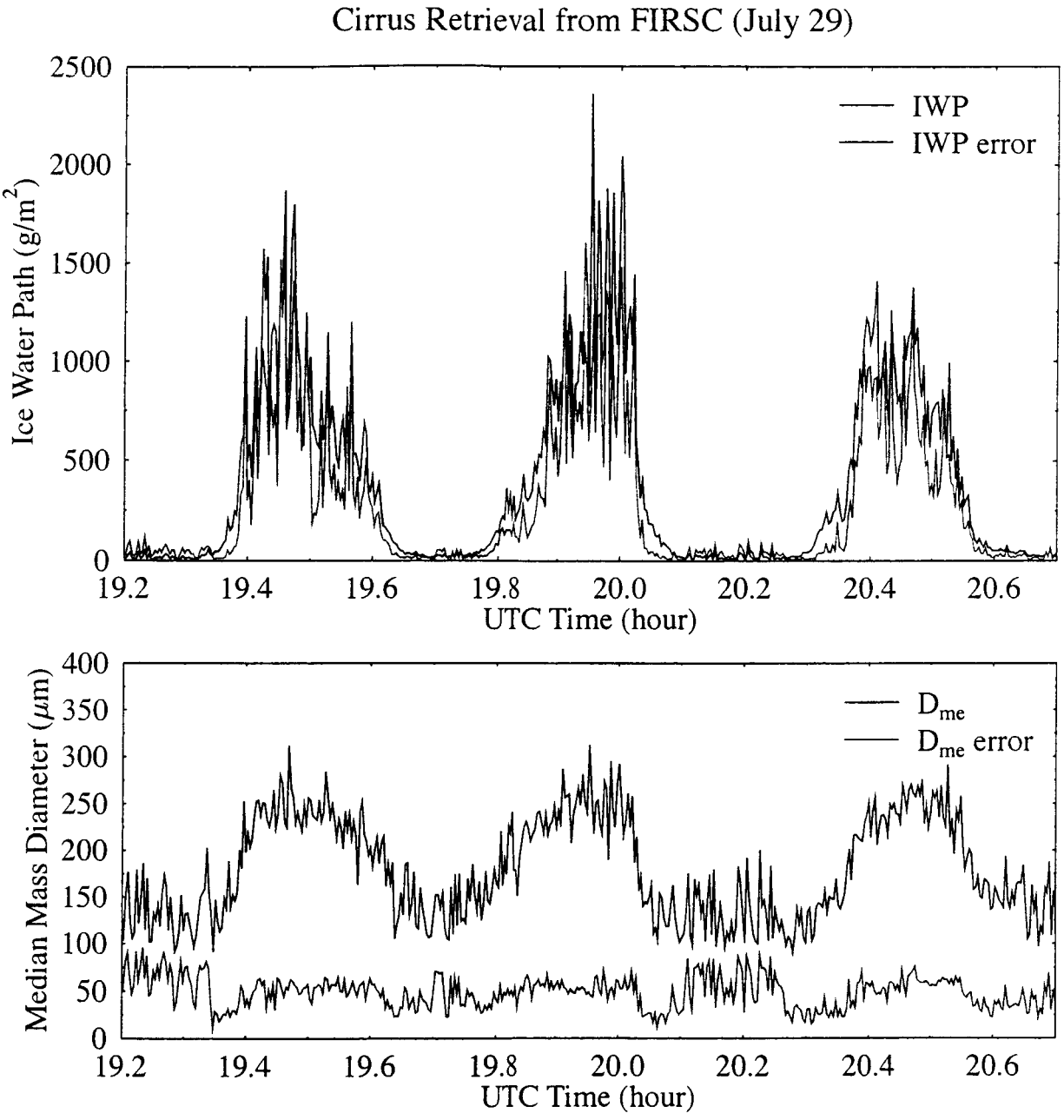

Figure 8: Retrievals of ice water path and particle size from FIRSC for a portion of the July 29 flight. The errors are one standard deviation uncertainties from the Bayesian retrieval algorithm.